Journal of Membrane Science 581 (2019) 413–420

Contents lists available at ScienceDirect

Journal of Membrane Science

journal homepage: www.elsevier.com/locate/memsci

Controlling pore structure of polyelectrolyte multilayer nanofiltration membranes by tuning polyelectrolyte-salt interactions

Ryan M. DuChanois, Razi Epsztein, Janvi A. Trivedi, Menachem Elimelech*

Department of Chemical and Environmental Engineering, Yale University, New Haven, CT, 06520-8286, USA

ARTICLE INFO

Keywords:
Pore size
Layer-by-layer assembly
Charge compensation
Ion selectivity
Membrane thickness

ABSTRACT

Nanofiltration membranes have limited ion-ion selectivity in water treatment applications, especially when separating ions with similar size and charge. To achieve greater size-based selectivity in nanofiltration, more control of pore structure is required during membrane fabrication. We demonstrate how to tailor membrane pore size and thickness using polyelectrolyte layer-by-layer assembly by alternately applying two strong polyelectrolytes, PDADMAC and PSS, to a polysulfone substrate while systematically controlling the polyelectrolyte and salt concentrations in the deposition solution. Results suggest that increasing polyelectrolyte concentration or salt concentration in the deposition solution increases polyelectrolyte multilayer thickness, but the effects on pore size may be categorized into two distinct regimes. In the first growth regime, increasing polyelectrolyte concentration in the deposition solution led to larger polymer deposition rates and smaller pore sizes. In the second growth regime, increasing polyelectrolyte concentration produced larger pore sizes. We attribute the second regime to less adsorbed polyelectrolyte on the membrane and/or less coiled polymer chains as a result of changing polyelectrolyte-salt interactions. Overall, results show that pore size modification is achievable using layer-by-layer assembly by tuning polyelectrolyte-salt interactions and can be used to study and improve size-based selectivity in membrane separation processes.

1. Introduction

Nanofiltration (NF) is a low-pressure membrane process that separates solutes from solvents [1–3]. Compared to reverse osmosis membranes, which remove almost all contaminants from solution, NF membranes have a less dense polymer structure that partially reject solutes, primarily by steric (size) and Donnan (charge) exclusion [4–8]. Species with larger hydrated radii than the pore are retained by the membrane [9], while the membrane charge plays a role in ion rejection by electrostatically repelling co-ions and attracting counterions [10]. Therefore, these intrinsic rejection mechanisms limit the ability for NF membranes to separate species of similar size and charge. To improve steric-based selectivity in NF, more precise control of membrane pore structure may be required to cater to size and shape of specific solutes.

Interfacial polymerization (IP) is the most common scalable technique for fabricating ultra-thin selective membrane layers [11,12]. In IP, the polymerization reaction occurs at the interface of two reactive monomers in immiscible liquids [13,14], traditionally between a diamine in an aqueous solution and a trimesoyl chloride in an organic solvent [15]. IP can be conducted with a range of monomers to fabricate membranes with high rejection but low resistance to water transport, aiding to its widespread application [16]. However, traditional IP provides limited control of membrane pore structure (e.g., thickness and pore size), which is critical for understanding solute transport and ultimately improving selectivity in membrane separations [17].

Another technique for fabricating membrane selective layers is polyelectrolyte layer-by-layer (LbL) assembly. LbL assembly is a bottom-up cyclical process where polycations and polyanions in solution are sequentially applied to a substrate; then, each stage is followed by rinsing to remove weakly associated polymers [18,19]. Polyelectrolyte multilayer (PEM) assembly is driven by electrostatic interactions between oppositely charged polyelectrolytes as well as entropy gain from polyelectrolytes releasing counterions and hydrating molecules [20,21]. A range of parameters in LbL assembly affect the PEM composition and structure, especially those of the deposition solution such as ionic strength [22–24], polyelectrolyte properties [25,26], polyelectrolyte concentration [22], pH [27–29], and temperature [30,31]. Thus, LbL assembly is a versatile method that enables the selection of appropriate deposition conditions to create a desired membrane structure [32]. Compared to IP, the LbL method is a unique platform for examining mechanisms of ion transport because of the ability to

* Corresponding author.
E-mail address: menachem.elimelech@yale.edu (M. Elimelech).

https://doi.org/10.1016/j.memsci.2019.03.077
Received 24 January 2019; Received in revised form 22 March 2019; Accepted 25 March 2019
Available online 27 March 2019
0376-7388/

systematically tailor the morphology of the membrane active layer [33].

Of the fabrication parameters in LbL assembly, the background ionic strength of the deposition solution has shown to play a particularly important role in determining PEM properties and performance [34]. Salt counterions screen charges along each polyelectrolyte chain, thereby decreasing self-repulsion between charged groups on the same chain and causing coiled polyelectrolyte conformations [35,36]. Further, salt counterions decrease electrostatic repulsion between polyelectrolytes of like charges, which allows polyelectrolytes to approach each other more closely and a greater amount of polyelectrolyte to adsorb on the membrane [23,35–37]. The background ionic strength of the deposition solution also dictates whether polyelectrolyte charges on the membrane surface mostly interact with oppositely charged polyelectrolytes or salt counterions. At low ionic strength, polyelectrolyte charges are primarily neutralized by oppositely charged polyelectrolytes (i.e., intrinsic compensation). Conversely, at high ionic strength, polyelectrolyte charges become primarily neutralized by salt counterions (i.e., extrinsic compensation) [22,38]. Extrinsic compensation leads to weaker attraction between polyelectrolytes and results in thicker PEMs [37–40].

For NF membranes, the active layer thickness and pore size determine membrane selectivity for uncharged solutes as well as water permeability [41,42]. As such, improving steric-based selectivity requires an ability to tailor both membrane thickness and pore size during fabrication. For the LbL fabrication process, the effect of a single deposition parameter (e.g., ionic strength or polyelectrolyte concentration) on the resulting PEM structure has been extensively studied, but the coupled effect of such parameters has not been well defined. More specifically, the role of the interplay between polyelectrolyte and salt in controlling membrane pore size and thickness is not well characterized.

In this study, we investigate how the deposition conditions in LbL assembly affect pore structure of nanofiltration membranes. We alternately applied two strong oppositely charged polyelectrolytes—poly (diallyldimethylammoniumchloride) (PDADMAC) and polyanionic poly (sodium 4-styrenesulfonate) (PSS)—on polysulfone substrates to fabricate nanofiltration membranes. We first evaluated how altering the background ionic strength (NaCl) and polyelectrolyte (PDADMAC and PSS) concentration in the deposition solution affect membrane solute rejection and water flux. Then we demonstrate how the polyelectrolyte and salt concentrations in the deposition solution influence PEM pore size and thickness, while discussing the intermolecular interactions underlying the resulting structure. Our findings highlight the ability to tailor pore structure using LbL assembly, which may be used to study solute transport and improve steric-based selectivity in membrane separation processes.

2. Materials and methods

2.1. Materials and chemicals

Polysulfone (PSf) ultrafiltration (UF) membranes (Sepro Membranes, Oceanside, CA, USA) with a 20 kDa molecular weight cut-off were utilized as the substrate for LbL assembly. Polycationic poly (diallyldimethylammoniumchloride) (PDADMAC; MW 150,000–200,000 g mol^{-1}; 20% wt. in water), polyanionic poly (sodium 4-styrenesulfonate) (PSS; MW 70,000 g mol^{-1}), erythritol (MW 122 g mol^{-1}), xylose (MW 150 g mol^{-1}), and glucose (MW 180 g mol^{-1}) were purchased from Sigma Aldrich (St. Louis, MO, USA). J.T. Baker Chemicals (Phillipsburg, NJ, USA) supplied sodium chloride (NaCl), isopropanol, and glycerol. Hydrochloric acid (HCl) was purchased from AmericanBio (Natick, Massachusetts, USA) and sodium hydroxide (NaOH) from Avantor (Center Valley, Pennsylvania, USA). UniversityWafer, Inc. (South Boston, MA, USA) provided silicon wafers (Mechanical Grade 1996). Deionized water (MilliPore, Billerica, MA, USA) was used for solution preparation, rinsing the membrane surface during LbL modification, and compacting the membranes.

2.2. Fabrication of nanofiltration membranes using LbL assembly

For LbL assembly, we pretreated a PSf UF membrane substrate in a 25% isopropanol solution for 30 min in a rotating shaker, followed by rinsing with deionized water for three 30-min cycles. The pristine PSf membrane was cut and placed in a specially designed frame with the active side facing up to allow its contact with the polyelectrolyte solutions. To modify the surface of the pristine membrane, we prepared aqueous polyelectrolyte solutions of PDADMAC and PSS with varying NaCl and polyelectrolyte concentrations (calculated based on monomer molar mass), which are specified in Section 3. PDADMAC and PSS are commonly used for LbL modification because they are strong polyelectrolytes and maintain their charge across operational pH values [7,11,41,43,44].

Unless noted otherwise, we first applied 10 mL of an aqueous cationic PDADMAC solution to the PSf substrate for 10 min. We then rinsed the membrane twice for 5 min using 10 mL NaCl solution (with equivalent ionic strength as the PDADMAC solution) to remove unadsorbed polyelectrolyte from the surface. Next, we applied 10 mL of anionic PSS solution to the cationic PDADMAC layer for 10 min, with two subsequent rinsing steps using 10 mL NaCl (with equivalent ionic strength as the PSS solution). The PDADMAC-PSS conjugation formed the first bilayer and we repeated this deposition cycle to form additional bilayers. All membranes terminated with the polyanion, PSS. We applied in total two bilayers to PSf substrates to evaluate membrane performance and estimate average pore size. For membrane thickness measurement, we used four bilayers on silicon wafers as described in Section 2.4. After assembly, we stored the modified PSf membranes in a glycerol/water (85% wt./15% wt.) solution for 4 h and then dried them overnight at room temperature [34]. Before use, membranes were rinsed thoroughly with DI water to remove the glycerol.

2.3. Nanofiltration system and solute rejection measurements

We determined solute rejection by the polyelectrolyte membranes in a custom, laboratory-scale crossflow system with membranes in plate-and-frame cells, with each flat sheet membrane coupon having an effective surface area of 20.02 cm^2. Water recirculated between the feed tank to the membrane cells at a crossflow velocity of 0.21 m s^{-1} and at a constant temperature of 25 ± 0.5 °C. Prior to filtration, we compacted membranes in the crossflow system overnight at an applied pressure of 10.3–13.8 bar (150–200 psi). After compaction, the applied pressure was reduced to 8.3 bar (120 psi) (unless otherwise noted), pure water flux was measured gravimetrically, and a concentrated stock solution was added to achieve a feed concentration of 50 mg L^{-1} total organic carbon (TOC) (glucose), 2 mM NaCl, or 1 mM Na_2SO_4. After waiting 30 min for stabilization, we collected feed and permeate samples to measure glucose concentration using a TOC analyzer (TOCV-CSH, Shimadzu Corp., Japan) or NaCl and Na_2SO_4 concentrations using an electrical conductivity meter (Oakton Instruments, Vernon Hills, IL). Rejection (R) was calculated for each prepared membrane using

$$R = \left(1 - \frac{C_p}{C_f}\right) \times 100\% \quad (1)$$

where c_p and c_f are the solute or salt concentrations in the permeate and feed, respectively.

2.4. Membrane characterization

We estimated NF membrane average pore sizes based on the hydrodynamic pore transport model, which assumes the membrane to be a bundle of cylindrical capillary tubes of the same radii. The model uses rejection data of neutral, inert organic tracers to calculate average

estimated pore sizes, as we described elsewhere [45]. We selected three neutral organic solutes with different molecular weight—erythritol (MW 122 g mol^{-1}), xylose (MW 150 g mol^{-1}), and glucose (MW 180 g mol^{-1})—to characterize the fabricated NF membranes. Using the crossflow system and experimental conditions described previously, we added a concentrated stock solution to the feed tank to achieve 50 mg L^{-1} TOC. Samples were collected from the feed and permeate solutions at operating pressures of 4.1, 6.2, 8.3, and 10.3 bar (60, 90, 120, and 150 psi). We measured solute feed and permeate concentrations (as TOC) to calculate solute rejection (Eq. (1)) and used the data in the hydrodynamic pore transport model to estimate the average pore size. Reported average pore sizes and standard deviations are based on rejection of erythritol, xylose, and glucose. Statistical differences between samples were determined by two-sided *t*-tests assuming unequal variances and reported as *p*-values. Further details about the pore transport model are available in the Supplementary material (SM).

To evaluate the effect of the deposition conditions on PEM thickness, we performed LbL fabrication on atomically smooth silicon wafers in a specially designed frame. Using a similar process as in Section 2.2, we alternately applied 1 mL of PDADMAC and PSS solution to the substrate for 10 min, along with two subsequent 5 min rinsing steps of 1 mL NaCl solution. To remain above the detection limit of atomic force microscopy (AFM), we fabricated 4 bilayers of PDADMAC-PSS on each substrate with varying concentrations of NaCl and polyelectrolyte (specified in Section 3). Samples were then rinsed with DI water, air-dried overnight, and scratched with a metal precision glide needle (18G × 1 in., Becton Dickson & Co., Franklin Lakes, NJ) without damaging the silicon wafer. We measured dry-state thickness using a Bruker Dimension FastScan AFM (Santa Barbara, California) equipped with a Bruker FastScan-B cantilever (5 nm tip radius) in ScanAsyst mode. We adjusted the cantilever tip to the edge of the scratch and captured a 10 μm × 10 μm AFM image at a scan rate of 3 Hz. We used the Section function in Nanoscope Analysis v1.9 (Bruker) to determine membrane cross-sectional thickness by comparing scratched and non-scratched surfaces. We reported thickness values from averaging measurements from two independent samples for each LbL condition (three measurements per sample). Statistical differences between samples were determined by two-sided *t* tests assuming unequal variances and reported as *p*-values.

Surface zeta potential was determined for the PSf UF membrane substrate to explain its affinity for PDADMAC. We calculated zeta potential using streaming potential measurements performed by an electro-kinetic analyzer (EKA, Brookhaven Instruments, Holtsville, NY, USA), as described elsewhere [46]. Zeta potential was determined at a background electrolyte (KCl) concentration of 1 mM and temperature of 25°C. The solution pH was adjusted using HCl and NaOH.

3. Results and discussion

3.1. Effect of polyelectrolyte and salt concentration on membrane performance

The goal of this study was to understand how changing deposition conditions in LbL assembly, specifically polyelectrolyte and salt concentration, may be used to tailor membrane pore structure. We fabricated PEM NF membranes by applying polyelectrolytes to pristine PSf UF membrane substrates with negative zeta potential (Fig. S1). Different membranes were prepared by systematically altering polyelectrolyte concentration and background ionic strength of the deposition solution. Our early experiments investigated the effect of changing polyelectrolyte and salt concentration in the LbL deposition solution on membrane water flux and glucose rejection (Fig. 1). Considering that glucose is uncharged, steric exclusion controlled glucose rejection by the NF membranes. Therefore, performance metrics such as water flux and glucose rejection are indicative of membrane characteristics such as membrane pore size and thickness.

At an NaCl concentration of 0.5 M, increasing polyelectrolyte concentration from 0.032 to 0.8 mM in the deposition solution produced NF membranes with decreasing water flux and increasing glucose rejection (Fig. 1A). This observation suggests that as greater polyelectrolyte concentration was applied to the membrane surface, there was greater resistance to water and solute transport due to the properties of the PEM (such as increased thickness or decreased pore size). However, when using polyelectrolyte concentrations higher than 0.8 mM during LbL assembly, the membrane water flux increased and glucose rejection decreased. This finding suggests that increasing polyelectrolyte concentration above a certain point increased membrane permeability to water and glucose, which can occur by decreasing membrane thickness or increasing pore size. We found similar rejection trends for independently fabricated membranes filtering feed solutions of 50 mg L^{-1} TOC (glucose) and 2 mM Na_2SO_4 at 5.5 bar (80 psi) (Fig. S2).

We also investigated the effect of the background ionic strength on membrane performance by fabricating membranes with varying salt concentrations of the LbL deposition solution while keeping the polyelectrolyte concentration constant (Fig. 1B). Initially, increasing background ionic strength of the deposition solution from 0.16 M to 1.25 M led to membranes with higher glucose rejection and lower water flux. These measurements can be explained by previous research on LbL assembly suggesting that as background ionic strength increases, polymer chains become more coiled and a greater amount of polyelectrolyte adsorbs to the membrane [23]. Increasing salt concentration also leads to extrinsic compensation of polyelectrolytes on the membrane surface, or weaker complexes between oppositely charged polyelectrolytes, that may produce thicker PEMs and can increase resistance to solute and water transport [38–40]. As we further increased the background ionic strength from 1.25 M to 2.5 M, the membrane rejection decreased as water flux increased. We found similar trends for water flux and glucose rejection for membranes independently fabricated at 10 mM polyelectrolyte concentration with varying background ionic strength in the deposition solution (Fig. S4). These findings indicate that saturating the system with salt can increase membrane permeability through possible pathways such as decreasing thickness or increasing pore size.

Using water flux and glucose rejection data as indicators of PEM structure, we observed two distinct PEM growth regimes that are dependent on polyelectrolyte and salt concentrations in the deposition solution. As more salt was added to the deposition solution, membrane glucose rejection increased to a maximum in the first regime and then decreased in the second regime (Fig. 1B). Notably, we also observed two distinct regimes when increasing the polyelectrolyte concentration of the deposition solution (Fig. 1A). In subsequent sections, we elucidate these regimes by investigating the coupled effect of polyelectrolyte and salt on membrane pore structure.

3.2. Characterization of the first growth regime for PEMs

To better understand the first growth regime—why an increase in polyelectrolyte concentration leads to higher glucose rejection and lower water flux—we fabricated a set of membranes with 0.5 mM polyelectrolyte concentration and 0.5 M background ionic strength (Fig. 2). We used 0.5 mM PDADMAC and PSS to remain within the first growth regime and varied the volume of deposition solution applied to the membrane or the deposition time. We then measured glucose rejection and water flux for each membrane and normalized those measurements to facilitate comparison between membranes of different intrinsic permeabilities and selectivities.

As the LbL deposition time increased beyond five minutes, normalized glucose rejection increased and normalized water flux decreased (Fig. 2A). This performance behavior indicates that the membrane average pore size decreased or the thickness increased with greater deposition time, which is supported by another study that found PEM thickness to increase with deposition time [22]. However,

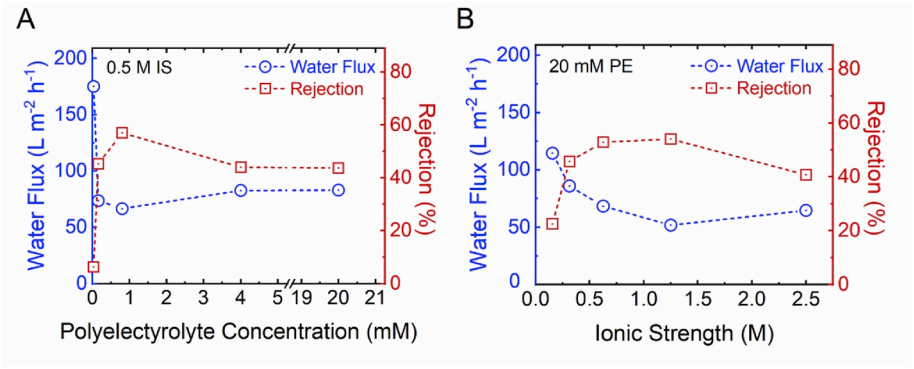

Fig. 1. Water flux and glucose rejection of LbL NF membranes fabricated with two bilayers of PDADMAC-PSS on PSf UF membrane supports at (A) 0.5 M background ionic strength (IS) with varying polyelectrolyte concentration (PE) and (B) 20 mM polyelectrolyte concentration with varying background ionic strength. Experimental conditions: glucose feed concentration of 50 mg L^{-1} as total organic carbon (TOC), applied pressure of 8.3 bar (120 psi), UF substrate glucose rejection of (A) 2.4% and (B) 0.3%, cross-flow velocity of 0.21 m s^{-1}, and temperature of 25 °C. Water flux was measured in the presence of glucose; pure water flux data is available in the SM (Fig. S3). Rejection of glucose was measured using a TOC analyzer. Polyelectrolyte concentration (mM) was calculated based on monomer molar mass.

increasing the volume of deposition solution while keeping polyelectrolyte concentration constant (increasing polyelectrolyte mass) did not increase the rate of polyelectrolyte transfer to the membrane surface (Fig. 2B). This evidence suggests that the membrane performance observed in the first growth regime, where an increase of polyelectrolyte concentration led to higher rejection and lower water flux, is a function of the rate of polymer transport to the membrane surface and not the mass of polyelectrolyte available. That is, higher polyelectrolyte concentrations lead to larger polymer deposition rates and result in more polyelectrolyte adsorption to the membrane surface.

3.3. Characterization of the second growth regime for PEMs

The second growth regime observed—where an increase in polyelectrolyte concentration led to lower glucose rejection and higher water flux—suggests that not only polyelectrolyte deposition affects membrane performance, but also an interplay between polyelectrolyte and salt. Membrane performance can give an indication of how polyelectrolyte-salt interaction affects membrane structure, but it cannot differentiate between changes in PEM pore size and thickness. Therefore, to explain the second growth regime, we characterized PEMs by evaluating their average pore size and thickness.

To measure thickness, we fabricated different PEM films on atomically smooth silicon wafers by systematically altering polyelectrolyte concentration and background ionic strength of the deposition solution. We scratched the PEM film using a precision glide needle and imaged PEM films using AFM (Figs. S5–S7). Then we scanned each side of the edge of the scratch to measure differences in thickness across PEM and silicon wafer surfaces (Fig. 3A). Large peaks in thicknesses near the scratch edge are likely accumulations of displaced polyelectrolyte induced by the scratch (Fig. 3B). Considering films were fabricated on silicon wafers in a dry state, AFM data are not reflective of PEM thicknesses on polymeric membranes but rather provide insight into how film thickness changes as a function of polyelectrolyte or salt concentration. As polyelectrolyte concentration in the deposition solution increased to 20 mM, the PEM thickness significantly increased ($p < 0.01$) (Fig. 3C). However, the films with the largest PEM thickness (20 mM PDADMAC-PSS) did not achieve the highest solute rejection and lowest water permeability (Fig. 1A). This finding indicates that the polyelectrolyte-salt interaction affected PEM pore size differently than thickness.

Based on rejection measurements of neutral organic solutes (erythritol, xylose, and glucose), we applied the hydrodynamic pore transport model (see SM) to estimate average pore sizes of membranes that were fabricated on PSf UF support layers with varying polyelectrolyte or salt concentrations in the deposition solution [45]. Results suggest that as the polyelectrolyte concentration increased in the LbL deposition solution from 0.032 mM to 0.80 mM, the average pore radius decreased to a minimum ($p = 0.20$) (Fig. 3C). As the polyelectrolyte concentration further increased to 20 mM, pore sizes began to increase ($p = 0.06$), indicating that regulating polyelectrolyte or salt concentration in the deposition solution can affect the interaction between the two species to change membrane average pore size as well as thickness. Notably, the 0.80 mM PDADMAC-PSS membrane had the smallest pore size, which corresponds with the membrane that had the maximum glucose rejection in Fig. 1A. For chloride on the other hand, rejection increased with increasing polyelectrolyte concentration up to 20 mM (Fig. S2). This behavior may be due to charge effects, which were not considered in this study, or because chloride (hydrated size of 0.66 nm) is smaller than glucose (0.86 nm) and sulfate (0.77 nm) and,

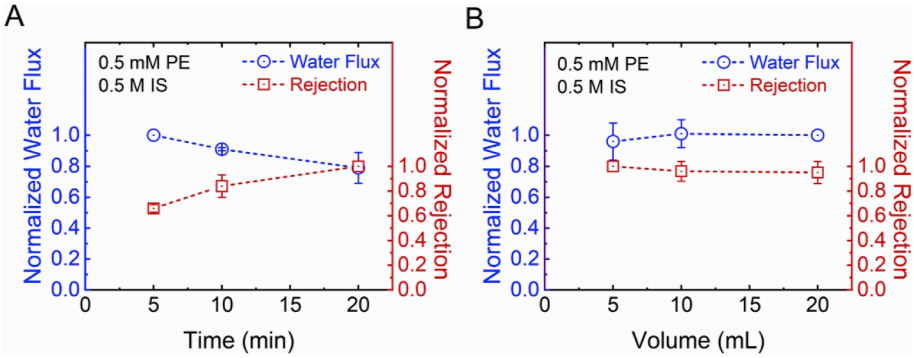

Fig. 2. Normalized pure water flux and glucose rejection of LbL NF membranes fabricated with two bilayers of 0.5 mM PDADMAC-PSS polyelectrolyte (PE) concentration and 0.5 M background ionic strength (IS) on PSf UF membrane supports. Normalized pure water flux and glucose rejection were calculated as a function of: (A) immersion time of membranes in polyelectrolyte deposition solution during fabrication (volume = 10 mL) and (B) volume of polyelectrolyte solution applied to UF support layer during fabrication (time = 10 min), where the lowest volume of deposition solution used (5 mL) was adequate to cover the membrane surface during fabrication. Normalized glucose rejection was calculated by dividing glucose rejection for each membrane by the glucose rejection for the membranes fabricated with (A) 20 min deposition time or (B) 5 mL deposition solution. Normalized pure water flux was calculated by dividing membrane water flux for each membrane by the water flux for the membranes fabricated with (A) 5 min deposition time or (B) 20 mL deposition solution. Experimental conditions: glucose feed concentration of 50 mg L^{-1} as total organic carbon (TOC), applied pressure of 8.3 bar (120 psi), UF substrate glucose rejection of 0.7%, cross-flow velocity of 0.21 m s^{-1}, and temperature of 25 °C. Rejection of glucose was measured using a TOC analyzer. Polyelectrolyte concentration (mM) was calculated based on monomer molar mass.

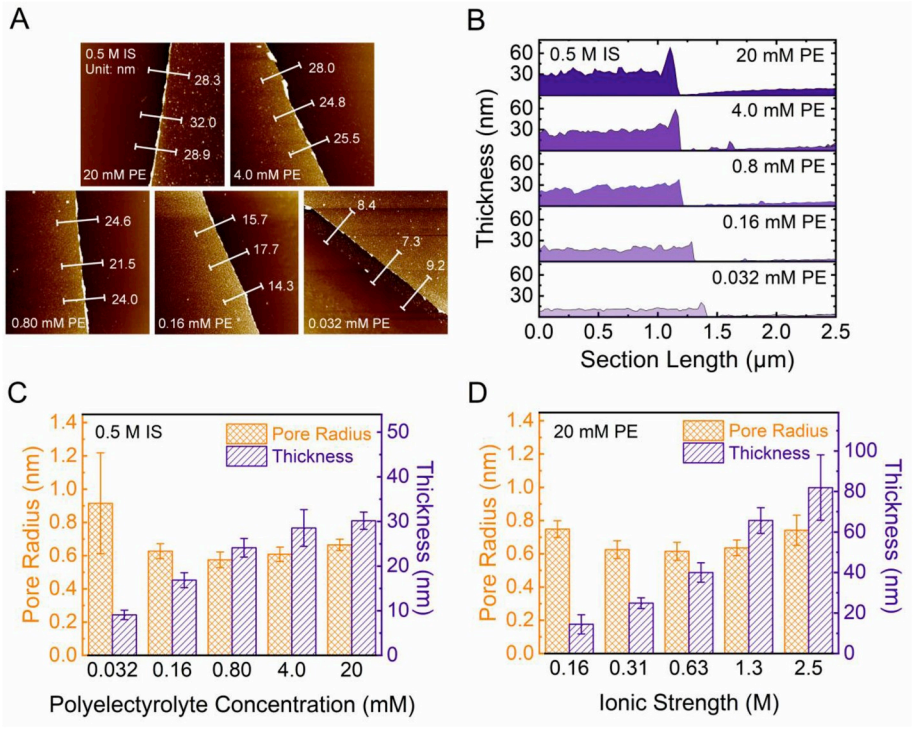

Fig. 3. (A) Sample AFM scans (10 μm × 10 μm) of four-bilayer dry-state films fabricated on silicon wafers at PDADMAC-PSS polyelectrolyte (PE) concentrations of 0.032, 0.16, 0.80, 4.0, and 20 mM with varying background ionic strength (IS). A scratch technique was used to measure thickness as the vertical displacement between the edge of the non-scratched and scratched surfaces (i.e., each side of the cross-cutting scratch) at three different positions. (B) Sample cross-sectional views of PEM thicknesses from AFM scans shown in (A). Thickness was measured as the vertical displacement between the non-scratched (left side) and scratched (right side) surfaces. Peaks in the profile near the scratch edge may be explained by the scratch displacing polyelectrolyte and causing accumulation of polyelectrolyte at the edge of the scratch. (C) Average estimated pore size and thickness for dry-state LbL PEMs fabricated at 0.5 M background ionic strength with varying polyelectrolyte concentration. (D) Average estimated pore size and thickness for dry-state LbL PEMs fabricated at 20 mM polyelectrolyte concentration with varying background ionic strength. Pore size was determined for membranes with two bilayers of PDADMAC-PSS on PSf UF membrane supports using rejection of erythritol, xylose, and glucose at applied pressures of 4.1, 6.2, 8.3, and 10.3 bar (60, 90, 120, and 150 psi). Experimental conditions: feed concentration of 50 mg L^{-1} as total organic carbon (TOC) for each sugar, cross-flow velocity of 0.21 m s^{-1}, and temperature of 25 °C. Rejection of glucose was measured using a TOC analyzer. Thickness was determined using AFM as described above and by averaging measurements from two separately prepared samples for each LbL condition (three measurements per sample). Polyelectrolyte concentration (mM) was calculated based on monomer molar mass.

therefore, can more easily fit into membrane pores [47,48].

We also characterized membranes that were fabricated with increasing salt concentrations in the deposition solution, while keeping the polyelectrolyte concentration constant (Fig. 3D). PEM films were fabricated on PSf UF substrates for pore size estimation and silicon wafers for thickness measurements. We observed similar trends for pore size and thickness as in Fig. 3C, albeit with greater thicknesses due to more extrinsic charge compensation in the PEM. That is, due to the increasing ionic strength, polyelectrolytes became more neutralized by hydrated salt counterions instead of oppositely-charged polyelectrolytes, which caused thicker deposited layers. As background ionic strength of the deposition solution increased from 0.16 M to 0.63 M, the average estimated pore size of the PEMs decreased to a minimum ($p = 0.04$), but at salt concentrations higher than 0.63 M, the average estimated pore size began to increase ($p = 0.13$) (Fig. 3D). The trend in pore sizes with increasing background ionic strength is broadly in agreement with water flux and solute rejection measurements presented earlier (Fig. 1B). PEM thicknesses significantly increased across the range of tested background ionic strengths ($p < 0.01$) (Fig. 3D and Fig. S8), similar to Fig. 3C.

Overall, results indicate that controlling polyelectrolyte or salt concentration of the deposition solution affects interactions between the two species to change PEM thickness, pore size, and, as a result, performance. In the following subsection, we further explore the role of polyelectrolyte-salt interactions in controlling membrane pore size and thickness and describe the potential mechanisms in effect.

3.4. Mechanisms of interaction between polyelectrolyte and salt

To further evaluate how the polyelectrolyte-salt interaction controls membrane structure, we fabricated and characterized membranes at higher ionic strength of 2.5 M NaCl in the deposition solution while varying polyelectrolyte concentration (Fig. 4) and compared them to membranes fabricated at 0.5 M NaCl (Figs. 1A and 3C). As before, PEM films were fabricated on PSf UF substrates for pore size estimations and silicon wafers for thickness measurements. The salt concentration was fivefold higher in the deposition solution (2.5 M NaCl), but water flux, solute rejection, pore size, and thickness trends were largely consistent with results for PEMs fabricated with 0.5 M NaCl. For both salt concentrations, the PEM thickness significantly increased as the polyelectrolyte concentration in the deposition solution increased to 20 mM ($p < 0.01$) (Fig. 4B and Fig. S9).

For pore size estimations, membranes fabricated with polyelectrolyte concentrations below 0.80 mM had average pore sizes that were too large to accurately estimate by the method utilized. At this low polyelectrolyte concentration, we surmise that limited amounts of polyelectrolyte deposited on the membrane surface and few polyelectrolyte-polyelectrolyte complexes were formed given the amount of salt in comparison to polyelectrolyte. Membrane average pore sizes then became smaller with increasing polyelectrolyte concentration up to 4.0 mM ($p = 0.08$). Increasing polyelectrolyte concentration above 4.0 mM led to larger pore sizes ($p = 0.05$), so there is similar relationship between polyelectrolyte concentration and pore size for both 2.5 M NaCl and 0.5 M NaCl experiments. More importantly, solute rejection was maximized and water flux and pore size were minimized for identical polyelectrolyte-salt ratios: 4 mM PDADMAC-PSS/2.5 M NaCl membrane (Fig. 4) and 0.8 mM PDADMAC-PSS/0.5 M NaCl membrane (Figs. 1A and 3C). These data suggest that to maximize solute rejection and minimize pore size for membranes fabricated with higher salt concentrations, higher polyelectrolyte concentrations are needed in the deposition solution. We explain this observation by polyelectrolyte and salt interacting via charge neutralization mechanisms to affect PEM properties and performance.

Charge neutralization (or compensation) occurs in the deposition solution by salt counterions screening opposite charges along polyelectrolyte chains. This screening phenomenon results in increased folding of polyelectrolyte chains due to reduced electrostatic repulsion between charged groups on monomer units [35,36]. For like

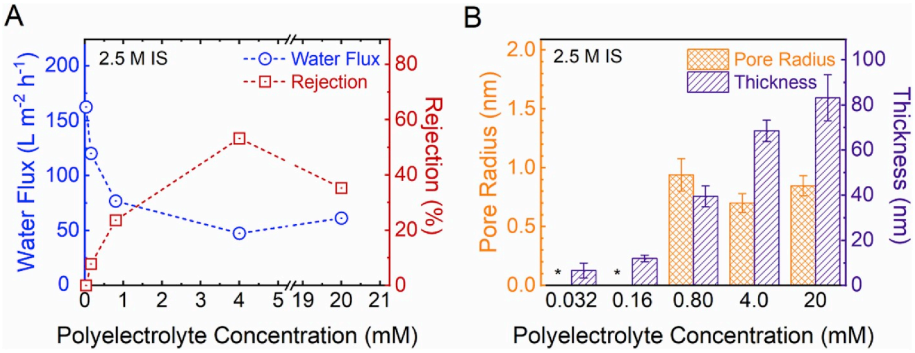

Fig. 4. (A) Water flux and glucose rejection of two-bilayer membranes fabricated on PSf UF membrane support layers at 2.5 M background ionic strength (IS) with varying PDADMAC-PSS polyelectrolyte (PE) concentration. Experimental conditions: glucose feed concentration of 50 mg L^{-1} as total organic carbon (TOC), applied pressure of 8.3 bar (120 psi), UF substrate glucose rejection of ~0%, cross-flow velocity of 0.21 m s^{-1}, and temperature of 25 °C. Water flux was measured in the presence of glucose; pure water flux data is available in the SM (Fig. S10). (B) Average estimated pore size and dry-state thickness for LbL PEMs fabricated at 2.5 M background ionic strength across a range of polyelectrolyte concentrations. Pore size was determined for membranes with two bilayers of PDADMAC-PSS on PSf UF membrane support layers using rejection of erythritol, xylose, and glucose at applied pressures of 4.1, 6.2, 8.3, and 10.3 bar (60, 90, 120, and 150 psi). Experimental conditions: feed concentration of 50 mg L^{-1} as total organic carbon (TOC), cross-flow velocity of 0.21 m s^{-1}, and temperature of 25 °C. Rejection of glucose was measured using a TOC analyzer. An asterisk (*) indicates pore sizes were too large to estimate with the method utilized. AFM was used to measure thickness of four-bilayer PDADMAC-PSS films on silicon wafers. Polyelectrolyte concentration (mM) was calculated based on monomer molar mass.

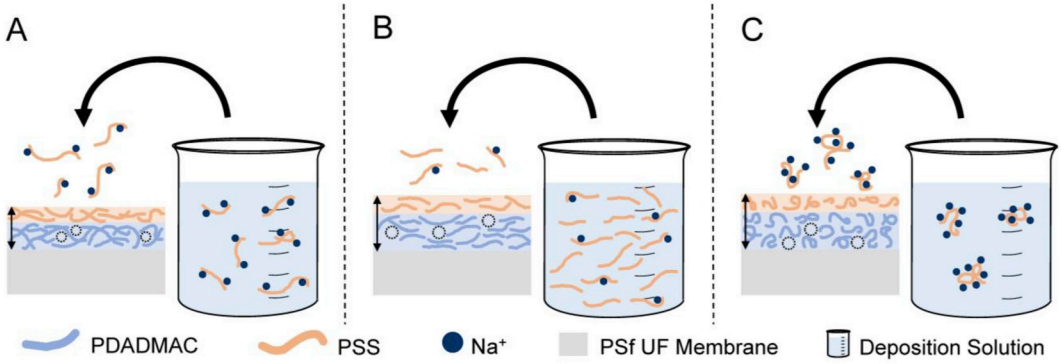

Fig. 5. Membrane pore structure is determined by the polyelectrolyte and salt concentrations of the deposition solution due to interactions between the polyelectrolyte and salt. (A) As a reference point, at some given polyelectrolyte and salt concentrations in the deposition solution, average estimated pore sizes are minimized. (B) With additional polyelectrolyte, PEM thickness and average estimated pore size increase. (C) With additional background ionic strength, PEM thickness and average estimated pore size increase. Sphere symbols represent salt counterions, blue chains are PDADMAC, orange chains are PSS, gray layers are polysulfone ultrafiltration substrates, and beakers represent the deposition solution. Co-ions as well as counterions in the PEM are not shown to emphasize PEM structure. (For interpretation of the references to colour in this figure legend, the reader is referred to the Web version of this article.)

polyelectrolytes, charge neutralization decreases electrostatic repulsion between polymer chains to increase mass adsorption on the membrane surface [23,35–37]. Salt counterions can also neutralize opposite charges on previously deposited polyelectrolyte layers to create weaker attraction between polyelectrolytes and thicker PEMs (i.e., extrinsic compensation) [37–40]. Importantly, data support that the polyelectrolyte concentration in the deposition solution also changes polyelectrolyte-salt interactions to control polymer complexation and conformation, which then affects PEM pore size and thickness.

The effects of polyelectrolyte-salt interactions on membrane pore structure are schematically presented (Fig. 5). As evident in Figs. 3 and 4, at some reference polyelectrolyte and salt concentrations in the deposition solution, pore sizes are minimized (Fig. 5A). Upon increasing polyelectrolyte concentration for a given deposition time, there is an increase in rate of polyelectrolyte deposition on the membrane surface, thus increasing layer thickness (Fig. 5B). Individual polymers are also statistically less likely to interact with salt counterions at higher polyelectrolyte concentrations. As a result, charged polyelectrolytes are less coiled in conformation, adsorb less to the membrane, and form more intrinsically compensated PEMs. We claim that these mechanisms in combination, or a subset of them, result in larger pores.

If, instead, the background salt concentration in the deposition solution increases (Fig. 5C), counterions screen more charges along each polyelectrolyte chain. The increase in thickness may be due to more extrinsic compensation, more polyelectrolyte adsorption on the membrane surface, and/or more coiled polyelectrolyte conformations. We attribute the increase in average pore size with higher salt concentration to more extrinsic compensation, which causes the PEM to become thicker and less dense. Additionally, charge interactions between oppositely charged polyelectrolytes on the membrane surface may screen salt ions to the extent that it limits polyelectrolyte adsorption, resulting in larger pores [23,37].

4. Conclusion

We demonstrate that controlling polyelectrolyte and salt concentrations in polyelectrolyte LbL assembly may be used to tune the pore structure of PEM NF membranes. Using AFM and the hydrodynamic pore transport model, we showed that increasing polyelectrolyte concentration or salt concentration in the deposition solution increased PEM thickness, but the effects on PEM average pore sizes were different for two distinct growth regimes. In the first growth regime, increasing polyelectrolyte and salt concentrations produced smaller pore sizes, which we attribute to larger polymer deposition rates and more adsorption of coiled polymers on the membrane surface, respectively. In the second growth regime, where additional polyelectrolyte or salt was added to the membrane surface, pore sizes increased, which we attribute to polyelectrolyte-salt charge neutralization interactions. More specifically, when increasing polyelectrolyte concentration, a decreasing proportion of charged monomers can be neutralized

by salt counterions, which results in less coiled polymer chains and less polyelectrolyte adsorption to the membrane. On the other hand, increasing salt concentration produces more extrinsically compensated PEMs that have thicker and less dense structures. Overall, our results highlight that pore size modification is achievable using LbL assembly for the polyelectrolytes and fabrication conditions in this study. Although controlling polyelectrolyte-salt interactions in LbL assembly also alters PEM thickness, an ability to fabricate membranes with tunable average pore sizes may enable fundamental transport studies on steric-based selectivity in membrane separation processes.

Acknowledgements

We acknowledge the support received from the National Science Foundation (NSF) through the Engineering Research Center for Nanotechnology-Enabled Water Treatment (EEC-1449500). Facilities used for AFM were supported by the Yale Institute of Nanoscale and Quantum Engineering (YINQE) under NSF MRSEC DMR 1119826. We also acknowledge the NSF Graduate Research Fellowship awarded to R.M.D. and the postdoctoral fellowship (to R. E.) provided from the United States-Israel Binational Agricultural Research and Development (BARD) Fund, Fellowship number FI-549-2016.

Appendix A. Supplementary data

Supplementary data to this article can be found online at https://doi.org/10.1016/j.memsci.2019.03.077.

References

[1] N. Hilal, H. Al-Zoubi, N.A. Darwish, A.W. Mohammad, M. Abu Arabi, A comprehensive review of nanofiltration membranes: treatment, pretreatment, modelling, and atomic force microscopy, Desalination 170 (2004) 281–308, https://doi.org/10.1016/j.desal.2004.01.007.
[2] J. Luo, Y. Wan, Effects of pH and salt on nanofiltration-a critical review, J. Membr. Sci. 438 (2013) 18–28, https://doi.org/10.1016/j.memsci.2013.03.029.
[3] S. Bhattacharjee, J.C. Chen, M. Elimelech, Coupled model of concentration polarization and pore transport in crossflow nanofiltration, AIChE J. 47 (2001) 2733–2745, https://doi.org/10.1002/aic.690471213.
[4] L.D. Nghiem, A.I. Schäfer, M. Elimelech, Role of electrostatic interactions in the retention of pharmaceutically active contaminants by a loose nanofiltration membrane, J. Membr. Sci. 286 (2006) 52–59, https://doi.org/10.1016/j.memsci.2006.09.011.
[5] B. Van Der Bruggen, A. Koninckx, C. Vandecasteele, Separation of monovalent and divalent ions from aqueous solution by electrodialysis and nanofiltration, Water Res. 38 (2004) 1347–1353, https://doi.org/10.1016/j.watres.2003.11.008.
[6] A.E. Childress, M. Elimelech, Relating nanofiltration membrane performance to membrane charge (electrokinetic) characteristics, Environ. Sci. Technol. 34 (2000) 3710–3716, https://doi.org/10.1021/es0008620.
[7] R. Epsztein, W. Cheng, E. Shaulsky, N. Dizge, M. Elimelech, Elucidating the mechanisms underlying the difference between chloride and nitrate rejection in nanofiltration, J. Membr. Sci. 548 (2017) 694–701.
[8] R. Epsztein, E. Shaulsky, N. Dizge, D.M. Warsinger, M. Elimelech, Role of ionic charge density in donnan exclusion of monovalent anions by nanofiltration, Environ. Sci. Technol. (2018), https://doi.org/10.1021/acs.est.7b06400 acs.est.7b06400.
[9] W.M. Deen, Hindered transport of large molecules in liquid-filled pores, AIChE J. 33 (1987) 1409–1425.
[10] A.E. Yaroshchuk, Non-steric mechanisms of nanofiltration: superposition of Donnan and dielectric exclusion, Separ. Purif. Technol. 22 (2001) 143–158.
[11] S.U. Baowei, T. Wang, Z. Wang, X. Gao, C. Gao, Preparation and performance of dynamic layer-by-layer PDADMAC/PSS nanofiltration membrane, J. Membr. Sci. 423–424 (2012) 324–331, https://doi.org/10.1016/j.memsci.2012.08.041.
[12] T. Tsuru, K. Ogawa, M. Kanezashi, T. Yoshioka, Permeation characteristics of electrolytes and neutral solutes through titania nanofiltration membranes at high temperatures, Langmuir 26 (2010) 10897–10905, https://doi.org/10.1021/la100791j.
[13] Y. Song, P. Sun, L.L. Henry, B. Sun, Mechanisms of structure and performance controlled thin film composite membrane formation via interfacial polymerization process, J. Membr. Sci. 251 (2005) 67–79, https://doi.org/10.1016/j.memsci.2004.10.042.
[14] P.W. Morgan, Interfacial polymerization, Encycl. Polym. Sci. Technol. (2011), https://doi.org/10.1002/0471440264.pst168.
[15] J.R. Werber, C.O. Osuji, M. Elimelech, Materials for next-generation desalination and water purification membranes, Nat. Rev. Mater. 1 (2016) 16018, https://doi.org/10.1038/natrevmats.2016.18.
[16] M.J.T. Raaijmakers, N.E. Benes, Current trends in interfacial polymerization chemistry, Prog. Polym. Sci. 63 (2016) 86–142, https://doi.org/10.1016/j.progpolymsci.2016.06.004.
[17] J.E. Gu, S. Lee, C.M. Stafford, J.S. Lee, W. Choi, B.Y. Kim, K.Y. Baek, E.P. Chan, J.Y. Chung, J. Bang, J.H. Lee, Molecular layer-by-layer assembled thin-film composite membranes for water desalination, Adv. Mater. 25 (2013) 4778–4782, https://doi.org/10.1002/adma.201302030.
[18] J.J. Richardson, M. Björnmalm, F. Caruso, Technology-driven layer-by-layer assembly of nanofilms, Science 348 (2015) aaa2491.
[19] J.J. Richardson, J. Cui, M. Björnmalm, J.A. Braunger, H. Ejima, F. Caruso, Innovation in layer-by-layer assembly, Chem. Rev. 116 (2016) 14828–14867, https://doi.org/10.1021/acs.chemrev.6b00627.
[20] J. Borges, J. Mano, Molecular interactions driving the layer-by-layer assembly of multilayers, Chem. Rev. 114 (2014) 8883–8942, https://doi.org/10.1021/cr400531v.
[21] K. Ariga, J.P. Hill, Q. Ji, Layer-by-layer assembly as a versatile bottom-up nanofabrication technique for exploratory research and realistic application, Phys. Chem. Chem. Phys. 9 (2007) 2319–2340, https://doi.org/10.1039/b700410a.
[22] S.T. Dubas, J.B. Schlenoff, Factors controlling the growth of polyelectrolyte multilayers, Macromolecules 32 (1999) 8153–8160, https://doi.org/10.1021/ma981927a.
[23] R.V. Klitzing, Internal structure of polyelectrolyte multilayer assemblies, Phys. Chem. Chem. Phys. 8 (2006) 5012–5033, https://doi.org/10.1039/b607760a.
[24] M. Lösche, J. Schmitt, G. Decher, W.G. Bouwman, K. Kjaer, Detailed structure of molecularly thin polyelectrolyte multilayer films on solid substrates as revealed by neutron reflectometry, Macromolecules 31 (1998) 8893–8906, https://doi.org/10.1021/ma980910p.
[25] J. Choi, M.F. Rubner, Influence of the degree of ionization on weak polyelectrolyte multilayer assembly, Macromolecules 38 (2005) 116–124, https://doi.org/10.1021/ma048596o.
[26] P. Kujawa, P. Moraille, J. Sanchez, A. Badia, F.M. Winnik, Effect of molecular weight on the exponential growth and morphology of hyaluronan/chitosan Multilayers: a surface plasmon resonance spectroscopy and atomic force microscopy investigation, J. Am. Chem. Soc. 127 (2005) 9224–9234, https://doi.org/10.1021/ja044385n.
[27] P. Bieker, M. Schönhoff, Linear and exponential growth regimes of multilayers of weak polyelectrolytes in dependence on pH, Macromolecules 43 (2010) 5052–5059, https://doi.org/10.1021/ma1007489.
[28] S.S. Shiratori, M.F. Rubner, pH-dependent thickness behavior of sequentially adsorbed layers of weak polyelectrolytes, Macromolecules 33 (2000) 4213–4219, https://doi.org/10.1021/ma991645q.
[29] D. Yoo, S.S. Shiratori, M.F. Rubner, Controlling bilayer composition and surface wettability of sequentially adsorbed multilayers of weak polyelectrolytes, Macromolecules 31 (1998) 4309–4318, https://doi.org/10.1021/ma9800360.
[30] M. Salomäki, I.A. Vinokurov, J. Kankare, Effect of temperature on the buildup of polyelectrolyte multilayers, Langmuir 21 (2005) 11232–11240, https://doi.org/10.1021/la051600k.
[31] H.L. Tan, M.J. McMurdo, G. Pan, P.G. Van Patten, Temperature dependence of polyelectrolyte multilayer assembly, Langmuir 19 (2003) 9311–9314, https://doi.org/10.1021/la035094f.
[32] M.L. Bruening, D.M. Dotzauer, P. Jain, L. Ouyang, G.L. Baker, Creation of functional membranes using polyelectrolyte multilayers and polymer brushes, Langmuir 24 (2008) 7663–7673.
[33] C. Cheng, A. Yaroshchuk, M.L. Bruening, Fundamentals of selective ion transport through multilayer polyelectrolyte membranes, Langmuir 29 (2013) 1885–1892, https://doi.org/10.1021/la304574e.
[34] J. de Grooth, R. Oborný, J. Potreck, K. Nijmeijer, W.M. de Vos, The role of ionic strength and odd-even effects on the properties of polyelectrolyte multilayer nanofiltration membranes, J. Membr. Sci. 475 (2015) 311–319, https://doi.org/10.1016/j.memsci.2014.10.044.
[35] S. Bharadwaj, R. Montazeri, D.T. Haynie, Direct determination of the thermodynamics of polyelectrolyte complexation and implications thereof for electrostatic layer-by-layer assembly of multilayer films, Langmuir 22 (2006) 6093–6101, https://doi.org/10.1021/la0518391.
[36] M. Schönhoff, Layered polyelectrolyte complexes: physics of formation and molecular properties, J. Phys. Condens. Matter 15 (2003) R1781–R1808, https://doi.org/10.1088/0953-8984/15/49/R01.
[37] B. Schoeler, G. Kumaraswamy, F. Caruso, Investigation of the influence of polyelectrolyte charge density on the growth of multilayer thin films prepared by the layer-by-layer technique, Macromolecules 35 (2002) 889–897, https://doi.org/10.1021/ma011349p.
[38] N. Joseph, P. Ahmadiannamini, R. Hoogenboom, I.F.J. Vankelecom, Layer-by-layer preparation of polyelectrolyte multilayer membranes for separation, Polym. Chem. 5 (2014) 1817–1831, https://doi.org/10.1039/C3PY01262J.
[39] J.B. Schlenoff, S.T. Dubas, Mechanism of polyelectrolyte multilayer growth: charge overcompensation and distribution, Macromolecules 34 (2001) 592–598, https://doi.org/10.1021/ma0003093.
[40] X. Li, W. Goyens, P. Ahmadiannamini, W. Vanderlinden, S. De Feyter, I. Vankelecom, Morphology and performance of solvent-resistant nanofiltration membranes based on multilayered polyelectrolytes: study of preparation conditions, J. Membr. Sci. 358 (2010) 150–157, https://doi.org/10.1016/j.memsci.2010.04.039.
[41] R. Malaisamy, A. Talla-Nwafo, K.L. Jones, Polyelectrolyte modification of nanofiltration membrane for selective removal of monovalent anions, Separ. Purif. Technol. 77 (2011) 367–374, https://doi.org/10.1016/j.seppur.2011.01.005.
[42] S.U. Hong, R. Malaisamy, M.L. Bruening, Separation of fluoride from other

monovalent anions using multilayer polyelectrolyte nanofiltration membranes, Langmuir 23 (2007) 1716–1722, https://doi.org/10.1021/la061701y.
[43] W. Cheng, C. Liu, T. Tong, R. Epsztein, M. Sun, R. Verduzco, J. Ma, M. Elimelech, Selective removal of divalent cations by polyelectrolyte multilayer nanofiltration membrane: role of polyelectrolyte charge, ion size, and ionic strength, J. Membr. Sci. 559 (2018) 98–106, https://doi.org/10.1016/j.memsci.2018.04.052.
[44] M.D. Miller, M.L. Bruening, Correlation of the swelling and permeability of polyelectrolyte multilayer films, Chem. Mater. 17 (2005) 5375–5381, https://doi.org/10.1021/cm0512225.
[45] L.D. Nghiem, A.I. Schäfer, M. Elimelech, Removal of natural hormones by nanofiltration membranes: measurements, modeling, and mechanisms, Environ. Sci. Technol. 38 (2004) 1888–1896, https://doi.org/10.1021/es034952r.
[46] S.L. Walker, S. Bhattacharjee, E.M.V. Hoek, M. Elimelech, A novel asymmetric clamping cell for measuring streaming potential of flat surfaces, Langmuir 18 (2002) 2193–2198, https://doi.org/10.1021/la011284j.
[47] R. Netrabukkana, K. Lourvanij, G.L. Rorrer, Diffusion of glucose and glucitol in microporous and mesoporous silicate/aluminosilicate catalysts, Ind. Eng. Chem. Res. 35 (1996) 458–464.
[48] E.R. Nightingale Jr., Phenomenological theory of ion solvation. Effective radii of hydrated ions, J. Phys. Chem. 63 (1959) 1381–1387.